Raman spectra of isotopic GaN

J. M. Zhang, T. Ruf, and M. Cardona
Max-Planck-Institut für Festkörperforschung, Heisenbergstrasse 1, D-70569 Stuttgart, Germany

O. Ambacher and M. Stutzmann
Walter Schottky Institut, Technische Universität München, Am Coulombwall, D-85748 Garching, Germany

J.-M. Wagner and F. Bechstedt
Friedrich-Schiller-Universität, Institut für Festkörpertheorie und Theoretische Optik, Max-Wien-Platz 1, D-07743 Jena, Germany
(Received 19 August 1997)

First-order Raman spectra of wurtzite GaN made from natural Ga and isotopically pure ^{15}N and natural N (99.63% ^{14}N) were measured at low temperature. The Raman frequencies of the polar optical phonons [A_1(TO, LO), E_1(TO,LO)] shift according to the inverse square root of the reduced masses, as expected. The isotope shifts of the two nonpolar E_2 modes deviate significantly from the reduced-mass behavior as well as from the dependence expected for pure N or Ga vibrations which might be expected in view of their large frequency difference. This indicates that the E_2 modes involve mixed Ga and N vibrations. From fits to the experimental data with a coupled two-mode model we determine the mode eigenvectors. They confirm the results of an *ab initio* calculation which we have done for the zone-center vibrations of wurtzite GaN. Our calculations also predict a vanishing coupling between the two B_1 silent modes. We also measured a $^{nat}Ga^{14}N_{0.5}{}^{15}N_{0.5}$ alloy sample. Additional negative frequency shifts due to isotope disorder are observed for the A_1(TO), E_1(TO), and the high-frequency E_2 modes as compared to the reduced-mass or coupled-mode behavior. An estimate from second-order perturbation theory provides a quantitative explanation of this result. [S0163-1829(97)05346-0]

I. INTRODUCTION

GaN and some other nitrogen-based III-V semiconductors have been at the focus of intensive studies in recent years due to their unique electronic and mechanical properties.[1] These materials, with a direct wide band-gap and high thermal stability, are now being used to make blue-to-ultraviolet light emitting devices and high-temperature electronics.[2] However, in spite of the technological perspectives of the III-V nitrides, little work has been performed on the fundamental properties of the materials compared to other III-V semiconductors.

Semiconductors made from pure stable isotopes can be used to investigate the influence of the average atomic mass on the lattice-dynamical properties (e.g., phonon frequencies, linewidths and lifetimes, lattice parameters, thermal expansion, thermal conductivity), and the electronic structure, as well as the isotopic-disorder induced effects.[3] A considerable number of studies in elemental group-IV diamond-type semiconductors have been published during the last few years.[3–5] Recently these investigations have been extended to compounds.[6–8] In contrast to elemental crystals, the shifts of the phonon frequencies, when the constituent atoms of the compound are isotopically substituted, depend strongly on the vibrational eigenvectors. Therefore, the different phonon eigenstates exhibit different isotope shifts. In CuCl different isotope shifts with Cu and Cl substitution led to the identification of the anomalous TO phonon structure.[6,8] In wurtzite-type CdS, different isotope shifts have been found for polar and nonpolar optical modes.[7] While the polar phonons [A_1(TO,LO), E_1(TO,LO)] change with the reduced mass as expected, the high- and low-frequency nonpolar (but Raman-active) E_2 modes shift mainly, however not exactly, with the mass of either the S or the Cd atoms. Isotope substitution allowed us to determine the E_2-mode mixing and their eigenvectors in CdS.[7]

As already pointed out by Foreman and Lomer in 1957,[9] a complete lattice-dynamical description of a crystal requires the determination of phonon eigenvectors in addition to their eigenfrequencies. Inelastic neutron scattering is a suitable way to measure phonon eigenvectors and was previously utilized in Si and GaAs.[10,11] However, this technique requires an accurate measurement of scattering intensities, which is not always easy to achieve.

Using perturbation theory one can derive that the isotope shift of phonons in compounds is proportional to the squared magnitude of the corresponding atomic component of the eigenvectors:[12]

$$\frac{\partial \omega_n}{\partial M_i} = -\frac{\omega_n}{2M_i}\sum_{\alpha} |u_{i,\alpha}(n)|^2, \tag{1}$$

where ω_n is the frequency of mode n, M_i represents the mass of atom i, and $u_{i,\alpha}(n)$ gives the ith component of the orthonormal eigenvector of mode n along the direction α ($\alpha = x$, y, or z). By measuring the phonon frequency shifts induced by the change of the mass of a certain atom one can therefore obtain information about the corresponding phonon eigenvectors. In this work we present experimental and theoretical investigations of the effects in wurtzite GaN for different N isotopes. The experimental phonon frequencies and eigenvectors derived from these effects compare well with those obtained from first-principles lattice-dynamical calculations.

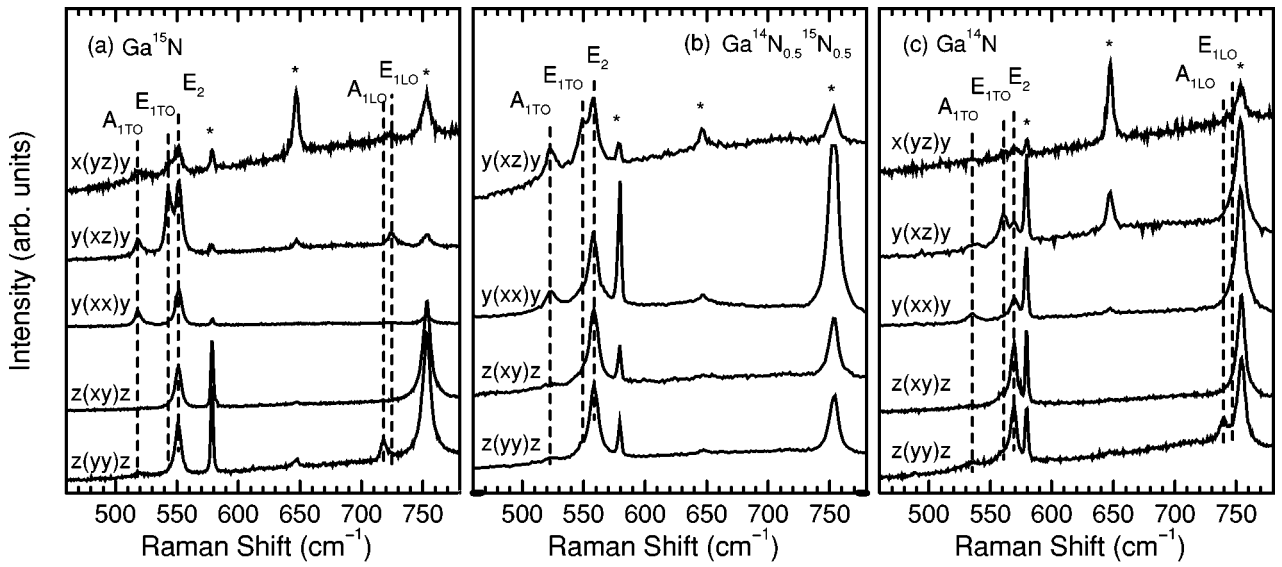

FIG. 1. Raman spectra of $Ga^{15}N$ (a), $Ga^{14}N_{0.5}{}^{15}N_{0.5}$ (b), and $Ga^{14}N$ (c), respectively. The spectra were taken at 10 K with 514.5 nm excitation using the scattering geometries indicated in the figure. Peaks marked by asterisks are phonons from the sapphire substrates.

Numerous studies have been performed also on isotopic-disorder effects in monoatomic crystals, such as Ge,[3,13] C,[3,14] α-Sn,[5] and C_{60}.[12] Disorder-induced resonant band modes[15] as well as additional frequency shifts and phonon linewidth broadenings have been observed in these systems. Calculations based on the coherent-potential approximation (CPA) give good agreement between experiment and theory. However, reports on isotopic-disorder effects in compound semiconductors are scarce.[8] In the present work, we use a $^{nat}Ga^{14}N_{0.5}{}^{15}N_{0.5}$ alloy sample with maximum mass disorder at the N sites for an investigation of these effects. Additional frequency shifts are observed for the A_1(TO), E_1(TO), and the high-frequency E_2 modes compared to those expected from the average mass in the alloy. A calculation based on second-order perturbation theory gives a qualitative and quantitative explanation of the results.

II. EXPERIMENT AND RESULTS

Isotopic GaN thin films were grown on *c*-axis oriented Al_2O_3 substrates with plasma-assisted molecular-beam-epitaxy (MBE) at a substrate temperature of 800 °C. The deposition rate was around 0.5 μm/h. The flux rates of the isotopically pure nitrogen (0.5% ^{14}N, 95.5% ^{15}N) plasma and natural gallium atoms were 10^{15} and 9.5×10^{14} cm^{-2} s^{-1}, respectively. A reference sample grown with natural gallium and natural nitrogen (99.634% ^{14}N,0.366% ^{15}N), which is denoted by ^{14}N in the following, and the $^{nat}Ga^{15}N_{0.5}{}^{14}N_{0.5}$ alloy sample were prepared under identical conditions. Atomic-force-microscopy measurements showed that all samples have a flat surface morphology. The measured free-carrier concentrations are $n=2\times10^{16}$, 1×10^{18}, and 2×10^{19} cm^{-3}, and the thicknesses of the layers are 1.0, 1.3, and 1.0 μm for the films of $^{nat}Ga^{15}N$, $^{nat}Ga^{14}N$, and the alloy sample, respectively. The accurate concentrations of N isotopes in the alloy sample were measured by secondary-ion-mass-spectroscopy as $[^{14}N]$ = (51.7 ± 2.0) % and $[^{15}N]$ = (48.2 ± 2.0) % and by elastic-recoil-detection-analysis[16] as $[^{14}N]=(54.0\pm0.5)$ % and $[^{15}N]=(46.0\pm0.5)$ %.

Raman spectra were recorded using a DILOR XY spectrometer equipped with a liquid-nitrogen-cooled charge-coupled-device detector. Either the 5145 Å line or the 4880 Å line of an Ar-ion laser was used to excite the samples, both lines are below the band-gap energy in the transparent region of GaN. Long accumulation times were necessary to measure the low-frequency E_2 modes since their intensities are rather weak. To obtain these phonon frequencies more accurately we recorded several spectra with slightly shifted spectrometer positions. A combination of these measurements results in spectra with effectively one data point every 0.5 cm^{-1}.

The samples were kept at 10 K in a closed-cycle helium cryostat to reduce the luminescence background. A laser power of about 50 mW, focused to a point (about 50 μm diameter), was used. Because both GaN and sapphire are transparent to the visible laser lines, sample heating is negligible. To observe all six Raman-active phonons propagating parallel or perpendicular to the uniaxial *c* axis (along the *z* direction, the growth direction in our samples), several right-angle or back-scattering geometries were selected, such as $z(yy)\bar{z}$ [for A_1(LO), E_2], $x(zx)y$ [E_1(LO,TO)], and $y(xx)\bar{y}$ [A_1(TO), E_2], etc.[7,17] For the polar modes in wurtzite crystals one has to keep in mind that mixed transverse and longitudinal phonons appear when the propagation directions are not exactly along the principal axes.[17,18] To avoid this direction-dispersion effect and to obtain the pure phonon frequencies, several measurements were made turning the sample by a small angle. Spectra for which a small rotation did not result in a frequency shift, i.e., for which direction dispersion was minimal, were used to determine the phonon frequency.

Figures 1(a), 1(b), and 1(c) show Raman spectra of $Ga^{15}N$, $Ga^{14}N_{0.5}{}^{15}N_{0.5}$, and $Ga^{14}N$, respectively, measured at 10 K in the frequency region between 460 and 780 cm^{-1}. Expanded regions of the high- and low-frequency E_2 modes

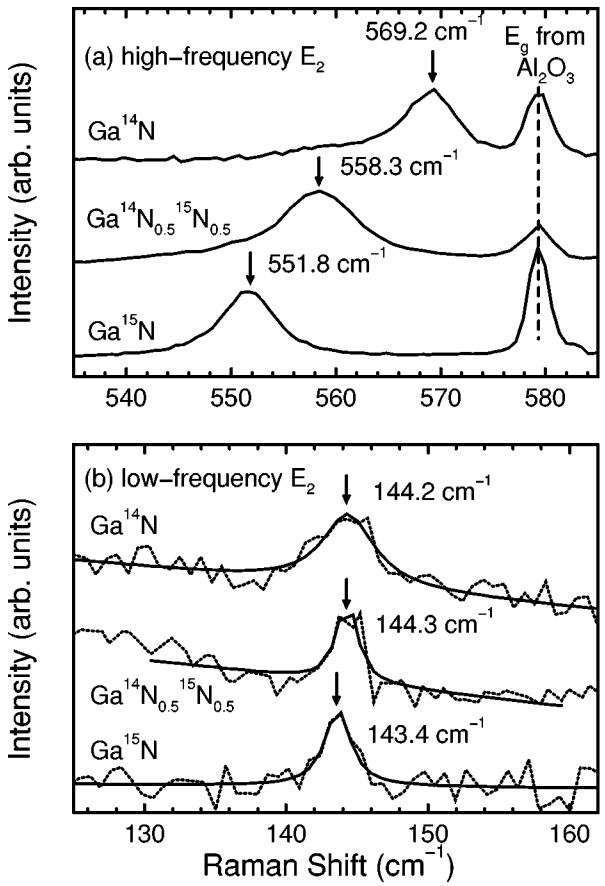

FIG. 2. Raman spectra of $Ga^{15}N$, $Ga^{14}N_{0.5}{}^{15}N_{0.5}$, and $Ga^{14}N$ in the energy region of high (a) and low frequencies (b), respectively. Spectra were taken at 10 K with 514.5 nm excitation in the $z(xy)\bar{z}$ configuration. The solid lines in (b) are fitted curves with Lorentzian profiles, while the dashed lines connect the data points of two measured spectra for each sample (see text).

are shown in Figs. 2(a) and 2(b), respectively. All Raman-active phonons, except for the two LO modes in the alloy sample, which has a high carrier concentration resulting in strong phonon-plasmon coupling, are observed in the scattering geometries given by the selection rules. Several E_g or A_{1g} modes from the sapphire substrate are also observed.[19] These lines are quite narrow and were used for calibration purposes. All Raman peaks were fitted with Lorentzian lineshapes. In Table I, we list the frequencies of all the modes observed in natural $Ga^{14}N$ and isotopic $Ga^{15}N$.

Numerous papers have been published recently dealing with strain-related phenomena in GaN thin films.[20,21] In pseudomorphically grown GaN films on the most commonly used substrates, such as sapphire and SiC, large strain is expected to be introduced because of the large lattice mismatch (-13% and 4%, for sapphire and SiC substrates, respectively) and different thermal-expansion coefficients. However, in our plasma-assisted MBE grown GaN films, no AlN buffer layer was generated prior to the growth of GaN with a nitridation of the sapphire substrates.[22] Under these conditions we believe that the strains due to lattice and thermal-expansion mismatch in our films are completely relaxed through the formation of dislocations.[23] This can be confirmed by comparing the Raman frequencies measured for the natural sample with the data measured on bulk GaN or strain-free GaN films on GaN substrates,[23–25] also listed in Table I. Furthermore, if there is any residual strain left it should be the same in $Ga^{15}N$ and $Ga^{14}N_{0.5}{}^{15}N_{0.5}$ as for the natural sample since all were grown under the same conditions with a comparable thickness. Thus, we do not need to take into account strain-induced frequency shifts (if any), which would be hard to separate from isotope shifts.

As shown in Table I, all the observed Raman modes exhibit prominent frequency shifts after the substitution of ^{15}N. However, the magnitudes of the shifts differ for different modes. For the polar optical modes, i.e., A_1(LO,TO) and E_1(LO,TO), within the experimental error bars the frequency ratios are equal to the inverse square root of the reduced mass ratio:

$$\frac{\omega(Ga^{15}N)}{\omega(Ga^{14}N)}=\sqrt{\frac{\mu(Ga^{14}N)}{\mu(Ga^{15}N)}}=0.9722, \tag{2}$$

TABLE I. Experimental Raman-active phonon frequencies for $Ga^{14}N$ and $Ga^{15}N$ at 10 K. Other experimental results for natural GaN are also listed.

Symmetry	$\omega(Ga^{14}N)$ (cm^{-1})		$\omega(Ga^{15}N)$ (cm^{-1})	$\frac{\omega(Ga^{15}N)}{\omega(Ga^{14}N)}$
	Present work	Others	Present work	
E_2(low)	144.2±0.5	142[a], 144[b], 144[c]	143.4±0.4	0.9945±0.0062
A_1(TO)	533.5±0.2	534[b], 531[c]	518.8±0.2	0.9724±0.0008
E_1(TO)	560.0±0.2	560[b], 560[c]	544.2±0.2	0.9718±0.0007
E_2(high)	569.2±0.2	566.5[a], 569[b], 568[c]	551.8±0.2	0.9694±0.0007
A_1(LO)	739.3±0.4	734[a]	719.2±0.2	0.9728±0.0008
E_1(LO)	746.6±0.8		725.3±0.4	0.9715±0.0013

[a]Reference 23: relaxed GaN films on GaAs or Al_2O_3, the TO and LO phonon from the GaAs substrate were at 266 and 291 cm^{-1}, respectively.

[b]Reference 24: bulk GaN, Raman at 20 K.

[c]Reference 25: bulk GaN, Raman at room temperature.

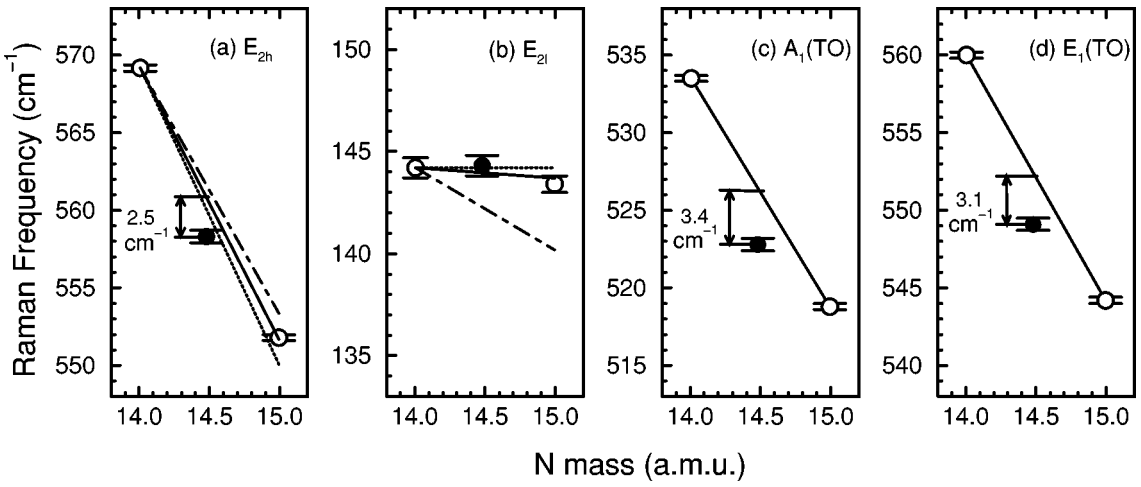

FIG. 3. Raman frequencies of the high- (a) and low-frequency (b) E_2, E_1(TO) (c), and A_1(TO) (d) modes versus the N isotope mass. The solid lines are predictions from Eq. (3) using the fitted parameters in Eq. (4) for the E_2 modes [(a) and (b)] and from $\omega \sim 1/\sqrt{\mu}$ for the A_1(TO) and E_1(TO) modes [(c) and (d)]. In (a) and (b), the predictions from the reduced-mass behavior are shown by the dashed-dotted lines. Expected shifts for the high- and low-frequency E_2 phonons as pure vibrations of N and Ga atoms, respectively, without mixing are represented by the dotted lines.

where $\mu^{-1} = m_{\text{cation}}^{-1} + m_{\text{anion}}^{-1}$, and the masses are calculated by using the actual atomic percentages of ^{14}N and ^{15}N in the samples.

For the two nonpolar E_2 modes the isotope-induced frequency shifts deviate significantly from the above-mentioned reduced-mass behavior. As can be seen clearly in Figs. 3(a) and 3(b), the frequency shift from ^{14}N to ^{15}N is larger (smaller) than that expected from the reduced-mass behavior (dashed-dotted line) for the high- (low-) frequency E_2 mode, respectively. These deviations are much larger than the error bars of the experimental data marked in the figure.

We show in Fig. 3 the Raman frequencies of the high- and low-frequency E_2, A_1(TO), and E_1(TO) modes in the Ga^{14}N$_{0.5}$^{15}N$_{0.5}$ alloy together with the data in the two isotopically pure samples. The alloy sample with large N-mass fluctuations has Raman frequencies which are lower than those expected from its average mass (solid lines). These additional frequency shifts are (-3.4 ± 0.7) cm^{-1}, (-3.1 ± 0.7) cm^{-1}, and (-2.5 ± 0.7) cm^{-1} for A_1(TO), E_1(TO), and the high-frequency E_2 mode, respectively. We attribute these shifts to a *mass disorder* effect.[3,13] No additional frequency shift, however, is observed for the low-frequency E_2 phonon.

III. CALCULATIONS AND DISCUSSIONS

A. Eigenvectors

Similar to CdS and ZnO, hexagonal GaN has a wurtzite structure possessing two formula units per primitive unit cell. Group theory predicts the following Γ-point optical phonon modes for the wurtzite structure (point group C_{6v}):[26] $A_1 + E_1 + 2E_2 + 2B_1$, which are all Raman active except for the silent B_1 modes. Figure 4 shows some vibrational eigenvectors of the four atoms in the unit cell. The direction of motion can be derived from group theory for all the optical phonons. Concerning the polar modes (A_1 and E_1), two Ga (N) atoms in the unit cell move in the same direction (and by the same amount since they are equivalent by symmetry). This allows us to determine the ratio of the Ga and N displacements just from center-of-mass invariance. However, for nonpolar modes (E_2 and B_1), which can be associated with the back-folded Brillouin-zone edge at the X point of

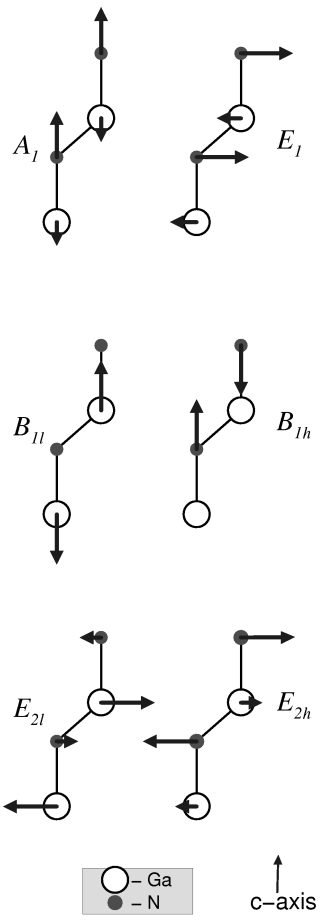

FIG. 4. Eigenvectors of the Γ-point optical phonons in wurtzite GaN. B_{1l} (E_{2l}) and B_{1h} (E_{2h}) correspond to the low- and high-frequency B_1 (E_2) modes, respectively.

TABLE II. Experimental and calculated Γ-point optical phonon frequencies (in cm^{-1}) and eigenvectors of nonpolar modes for $Ga^{14}N$. The relative signs of e_{Ga} and e_N cannot be obtained from the experiment. They are determined by the calculations.

Optical modes	Experiment		Calculation		
	Frequency	Eigenvector	Frequency		Eigenvector
			Present work	Others	
E_2(low)	144.2±0.5	$\lvert e_{Ga}\rvert$ = 0.677± 0.012 $\lvert e_N\rvert$ = 0.204± 0.045	143	146[a], 150[b]	e_{Ga} = 0.664 e_N = -0.242
A_1(TO)	533.5±0.2		541	534[a], 537[b]	
E_1(TO)	560.0±0.2		568	556[a], 555[b]	
E_2(high)	569.2±0.2	$\lvert e_{Ga}\rvert$ = 0.204± 0.045 $\lvert e_N\rvert$ = 0.677± 0.012	579	560[a], 558[b]	e_{Ga} = 0.242 e_N = 0.664
A_1(LO)	739.3±0.4		749		
E_1(LO)	746.6±0.8		757		
B_1(low)			338	335[a], 330[b]	e_{Ga} = 0.707 e_N = 0.028
B_1(high)			720	697[a], 677[b]	e_{Ga} = 0.028 e_N = -0.707

[a]Reference 35: linear muffin-tin orbitals.

[b]Reference 36: first-principles pseudopotential with mixed-basis approach.

the corresponding zinc-blende structure, the two Ga (N) atoms vibrate in antiparallel directions. Thus the eigenvectors of these two phonons cannot be derived from the above-mentioned simple feature. The magnitudes and signs of the atomic displacements for the E_2 and B_1 modes shown in Fig 4 are those either measured or calculated in the present work.

The two E_2 nonpolar normal modes of Ga and N can couple since they belong to the same representation of the C_{6v} group. In the harmonic approximation we can use a simple (but fully general for our purposes) phenomenological model to describe these two modes. Three force constants are used: the pure vibrations of N and Ga atoms in the unit cell are described by k_N and k_{Ga}, respectively, while the coupling is determined by the force constant k_{GaN}. Diagonalization of the dynamical matrix in the eigenvalue equation

$$\begin{pmatrix} -\omega^2+\dfrac{k_{Ga}}{m_{Ga}} & \dfrac{k_{GaN}}{\sqrt{m_{Ga}m_N}} \\ \dfrac{k_{GaN}}{\sqrt{m_{Ga}m_N}} & -\omega^2+\dfrac{k_N}{m_N} \end{pmatrix} \begin{pmatrix} e_{Ga} \\ e_N \end{pmatrix} = 0 \qquad (3)$$

yields the eigenvalues. Fitting these values to the experimental data, using a least-squares procedure, the three force constants are determined as

$$\begin{aligned} k_{Ga} &= (1.89\pm 0.33)\times 10^2 \ \text{N/m}, \\ k_N &= (2.47\pm 0.08)\times 10^2 \ \text{N/m}, \\ |k_{GaN}| &= (1.54\pm 0.32)\times 10^2 \ \text{N/m}. \end{aligned} \qquad (4)$$

The sign of k_{GaN} cannot be determined from this procedure, which implies that the relative sign of e_{Ga} and e_N cannot be obtained from these experiments. Note that the fit involves four experimental quantities (two frequencies and their slopes versus the isotopic mass of N) and three fit parameters, i.e., it is overdetermined. The fitted eigenvalues as a function of the N mass are represented by the solid lines in Figs. 3(a) and 3(b). Since there are four atoms in the unit cell and the two inequivalent cations (anions) vibrate with opposite phase but with identical magnitudes at the Γ point, eigenvector normalization requires

$$2(e_{Ga}^2+e_N^2)=1. \qquad (5)$$

With the obtained force constants, the eigenvector components e_{Ga} and e_N can be calculated. They are shown in Table II. These eigenvectors allow us to conclude that the low-frequency mode mostly involves the motion of Ga (with a Ga content of 92%, and a N admixture of 8%), while the high-frequency mode is dominated by the vibration of N atoms (with a N content of 92%, and a Ga admixture of 8%). This explains why the low-frequency E_2 mode (''Ga phonon'') hardly shifts while the high-frequency E_2 mode (''N phonon'') exhibits nearly the full isotope shift with N substitution.

An independent way to predict phonon frequencies and eigenvectors in crystals is based on lattice-dynamical model calculations, such as the rigid-ion, shell or bond-charge models. However, such calculations for the wurtzite structure are usually rather complicated due to the large number of adjustable parameters and the correctness of the corresponding eigenvectors is questionable without independent checks. Moreover, fitting procedures cannot be applied to most wurtzite crystals because only infrared and first-order Raman data exist, while neutron-scattering data are scare. This is the case especially for materials which contain Cd, such as CdS, because ^{113}Cd (natural abundance 12.2%) has a very large thermal neutron absorption cross section. Only very recently, a large ^{114}CdS sample was grown and the phonon-dispersion relations were measured.[28] In the case of GaN, high-quality samples can almost only be grown by thin-film deposition and experimental phonon-dispersion data are not available. On the other hand, even though an excellent agreement of the phonon frequencies between experiment and theory is often achieved, the associated eigenvectors usually differ

significantly.[11,32] Fortunately, the density-functional perturbation theory (DFPT) developed in recent years provides a powerful method to perform lattice-dynamical calculations.[27,33] Such parameter-free first-principles calculations have been used successfully for the accurate prediction of both phonon-frequencies and eigenvectors, not only for cubic but also for lower symmetry structures.[7,10,28–31]

We have performed such calculations within the framework of the density-functional theory (DFT) using the local-density approximation and a plane-wave pseudopotential method. The optical-phonon frequencies at the Γ point and the corresponding eigenvectors were obtained by solving the secular equation for the dynamical matrix. The pseudopotentials for Ga and N in our calculation were generated according to the scheme of Troullier and Martins[34] including the nonlinear core correction (NLCC) for the 3*d* states of Ga. Special effort is demanded in the conventional plane-wave calculation for nitrogen, since its pseudopotential is very deep, due to the lack of *p* electrons in the core, and thus the plane-wave expansion requires a high kinetic-energy cutoff (50 Ry) for good convergence. The Brillouin-zone integration was carried out using 12 Chadi-Cohen special points. Further details on the calculation can be found in Refs. 27 and 33.

Together with the experimental results, we list in Table II the calculated Γ-point phonon frequencies of all the optical modes and the corresponding eigenvectors of the nonpolar E_2 and B_1 vibrations. The data of two other calculations for GaN available are also listed.[35,36] The longitudinal vibration frequencies of polar modes were also obtained in our calculation by taking the long-range Coulomb interaction into account within DFPT in contrast to the frozen-phonon method.

Keeping in mind the accuracy of our first-principles calculations of 2%,[33] the calculated and measured frequencies agree very well with each other. The discrepancy between theory and experiment, however, is systematic, i.e., the calculated frequencies overestimate the experimental data by about 3%. We suggest that this tendency, which is nearly always present in phonon calculations using the NLCC approach,[28] is due, at least in part, to the NLCC approximation which takes *d* electrons frozen in the core, while in reality a non-negligible fraction of the *d* charge contributes to the bonds. Nevertheless, Karch *et al.* obtained a significant improvement of the agreement between the calculated and experimental lattice constant, high-frequency dielectric constant, and phonon frequencies by an inclusion of the 3*d* electron effects in cubic GaN using the NLCC approach.[33]

The *ab initio* predictions of the E_2 mode eigenvectors are in excellent agreement with the experiment. The mixing between the two E_2 vibrations is somewhat smaller than in CdS (17%).[7] This decrease of coupling from CdS to GaN can be attributed, at least in part, to the increase of the mass ratio from $m_{\mathrm{Cd}}/m_{\mathrm{S}} = 3.51$ to $m_{\mathrm{Ga}}/m_{\mathrm{N}} = 4.98$, which increases the energy difference between the two E_2 vibrations from 213 cm^{-1} in natural CdS to 425 cm^{-1} in natural GaN.

The mixing between the two B_1 modes in GaN, however, nearly vanishes. According to our calculation (see Table II), the high-frequency B_1 mode is almost a pure N vibration (with a Ga admixture of 0.2%) and the low-frequency B_1 mode a pure Ga vibration. Therefore, with an isotopic substitution of N the low-frequency B_1 mode should not shift, while the high-frequency B_1 mode should show the full N isotope shift. Unfortunately, measurements of these two silent modes are not available at present, and hence, the experimental determination of their eigenvectors is still an open task.

B. Isotopic disorder

In monoatomic crystals, the single-site CPA gives a good description of weakly disordered systems (e.g., mass-disordered).[5] The masses are considered complex and frequency dependent in terms of the dimensionless self-energy. This self-energy is determined from the self-consistency condition that the average scattering from a real atom embedded in the effective material must be zero. Using the phonon density of states generated in the virtual-crystal approximation, one can easily obtain the frequency-dependent self-energy and thus the disorder-induced frequency shift and broadening of the phonon linewidth which correspond to the real and imaginary part of the self-energy, respectively.

This calculation is more complicated in polyatomic crystals since mass fluctuations can exist at different atomic sites where the atoms have different eigenvectors. In addition, the phonon density of states of GaN with wurtzite structure, whose accuracy should be as high as possible when it is used in a CPA calculation, is not available at present. We performed a rough estimate of the disorder-induced frequency shifts from second-order perturbation theory while avoiding the full calculation in the following.

Applying perturbation theory to second order in such a system, one can obtain the mass-disorder-induced shift of the squared frequency (with respect to the average virtual crystal) from[12]

$$\Delta(\omega^2) = \omega^4 \int \frac{(\Delta M_{if})^2}{\omega^2 - \omega_i^2} N_d(\omega_i)\, d\omega_i , \tag{6}$$

where $\Delta M_{if} = [\mathbf{e_0(i)}/\sqrt{M_i}]\,\Delta\mathbf{M}\,[\mathbf{e_0(f)}/\sqrt{M_f}]$, in which $\Delta\mathbf{M}$ is the matrix of the mass fluctuations and $\mathbf{e_0}$ are the virtual-crystal eigenvectors. As shown in Fig. 4, for the high-frequency optical phonons, eigenvectors of N atoms are much larger than those of Ga atoms because the mass of Ga is much larger than that of N. These vibrations are mainly dominated by N atoms (with a Ga admixture of less than 17% for A_1(TO) and E_1(TO) and less than 10% for the high-frequency E_2). We make the reasonable approximation that the Ga atoms do not move and only the N atoms vibrate. In addition, we assume that the $\mathrm{Ga}^{14}\mathrm{N}_{0.5}{}^{15}\mathrm{N}_{0.5}$ alloy sample has only isotope disorder in the N sites, while there are no mass fluctuations on the Ga atomic sites. Further, we assume that mass fluctuations only occur at two equivalent atomic sites (there are totally four atoms) in the unit cell. These approximations simplify the mass-disorder problem in GaN to one similar as in the monoatomic diamond structures, and thus one obtains

$$\Delta\omega = g_2 \frac{\omega^3}{12} \int_0^\infty \frac{1}{\omega^2 - \omega_i^2} N_d(\omega_i)\, d\omega_i . \tag{7}$$

Normalization gives $\int_0^\infty N_d(\omega_i)d\omega_i = 12$, corresponding to the fact that there are 4×3 phonon states in the unit cell. The mass-fluctuation parameter is calculated with

$$g_2 = \sum x_i \left[1 - \frac{M_i}{\overline{M}}\right]^2, \tag{8}$$

where x_i is the concentration of the N isotope i, M_i is its mass, and $\overline{M}$ is the average nitrogen mass. In the approximations made above, g_2 is characterized only by N mass fluctuations without taking into account the atoms at the Ga sites. Equation (8) gives $g_2 = 1.2 \times 10^{-3}$ for the alloy sample. Unfortunately, as already mentioned above, the phonon density of states of GaN with wurtzite structure is not available at present. We therefore use the values from a first-principles calculation for zinc-blende GaN.[33] Proceeding in this fashion, the calculation yields an average disorder-induced shift $\Delta\omega = (-2.0 \pm 0.8)\ \mathrm{cm}^{-1}$ for the three optical phonons [A_1(TO), E_1(TO), and high-frequency E_2]. In contrast to Ge, C, and α-Sn where $\Delta\omega$ is positive, the N isotopic disorder in GaN causes a decrease of the phonon frequency. This is because the main part of the density of states, which effectively contributes to the frequency shifts, has an average frequency higher than those of the three modes. Considering the approximations made in this calculation, the value of $\Delta\omega$ is in reasonable agreement with the experiments [average value $(-3.0 \pm 0.7)\ \mathrm{cm}^{-1}$]. Concerning the low-frequency E_2 modes, which mostly involve vibrations of the Ga atoms (with a N admixture of less than 10%), the N isotopic disorder has no influence and thus no additional frequency shift can be observed.

IV. CONCLUSIONS

We have investigated the effect of ^{15}N isotopic substitution on the optical phonons in wurtzite GaN thin films using first-order Raman spectroscopy at low temperatures. While the observed phonon frequency shifts of the polar optical phonons [A_1(TO,LO), E_1(TO,LO)] follow, in the isotopically pure crystals, the inverse square root of the reduced mass, the behavior of the two nonpolar E_2 modes is quite different. The low-frequency E_2 mode hardly shifts, while the high-frequency vibration exhibits almost the full isotope shift. Fits to the experimental data with a coupled two-mode model yield the eigenvectors of these two modes and reveal a Ga (N) admixture to the high- (low-) frequency E_2 vibration of only 8%. The results of an *ab initio* calculation of the zone-center phonon frequency and eigenvectors are in good agreement with the observations.

Deviations between the experimental phonon frequencies and the average-mass behavior have been found for the three high-frequency optical modes in a $^{nat}Ga^{14}N_{0.5}{}^{15}N_{0.5}$ alloy sample where the isotopic disorder causes an additional shift of about $-3\ \mathrm{cm}^{-1}$. The magnitude and sign of this shift are supported by a calculation in second-order perturbation theory.

ACKNOWLEDGMENTS

J.M.Z. gratefully acknowledges financial support from the Max-Planck-Gesellschaft. Thanks are also due to A. Cantarero for a careful reading of the manuscript.

[1] F. A. Ponce and D. P. Bour, Nature (London) **386**, 351 (1997).
[2] S. Nakamura, Solid State Commun. **102**, 237 (1997).
[3] M. Cardona, in *Festköperprobleme: Advances in Solid State Physics*, edited by R. Helbig (Vieweg, Braunschweig, 1994), Vol. 34, p. 35.
[4] T. Ruf, H. D. Fuchs, and M. Cardona, Phys. Bl. **52**, 1115 (1996).
[5] D. T. Wang, A. Göbel, J. Zegenhagen, and M. Cardona, in *The Physics of Semiconductors*, edited by M. Scheffler and R. Zimmermann (World Scientific, Singapore, 1996), p. 197.
[6] T. Ruf, A. Göbel, M. Cardona, C. T. Lin, J. Wrzesinski, M. Steube, K. Reimann, N. Garro, A. Cantarero, J.-C. Merle, and M. Joucla, *The Physics of Semiconductors* (Ref. 5), p. 185.
[7] J. M. Zhang, T. Ruf, A. Göbel, A. Debernadi, R. Lauck, and M. Cardona, *The Physics of Semiconductors* (Ref. 5), p. 201.
[8] A. Göbel, T. Ruf, C. T. Lin, M. Cardona, J.-C. Merle, and M. Joucla, Phys. Rev. B **56**, 210 (1997).
[9] A. J. E. Forman and W. M. Lomer, Proc. Phys. Soc. London **70**, 1143 (1957).
[10] J. Kulda, D. Strauch, P. Pavone, and Y. Ishii, Phys. Rev. B **50**, 13 347 (1994).
[11] D. Strauch and B. Dorner, J. Phys. C **19**, 2853 (1986).
[12] J. Menéndez, J. B. Page, and S. Guha, Philos. Mag. B **70**, 651 (1994).
[13] M. Cardona, P. Etchegoin, H. D. Fuchs, and P. Molinás-Mata, J. Phys. Condens. Matter **5**, A61 (1993).
[14] J. Spitzer, P. Etchegoin, M. Cardona, T. R. Anthony, and W. F. Banholzer, Solid State Commun. **88**, 509 (1993).
[15] H. D. Fuchs, P. Etchegoin, M. Cardona, K. Itoh, and E. E. Haller, Phys. Rev. Lett. **70**, 1715 (1993).
[16] G. Dollinger, T. Faestermann, and P. Maier-Komor, Nucl. Instrum. Methods Phys. Res. B **64**, 422 (1992).
[17] C. A. Aguello, D. L. Rousseau, and S. P. Porto, Phys. Rev. **181**, 1351 (1969).
[18] L. Filippidis, H. Siegle, A. Hoffmann, C. Thomsen, K. Karch, and F. Bechstedt, Phys. Status Solidi B **198**, 621 (1996).
[19] S. P. S. Porto and R. S. Krishnan, J. Chem. Phys. **47**, 1009 (1967).
[20] F. Demangeot, J. Frandon, M. A. Renucci, O. Briot, B. Gil, and R. L. Aulombard, Solid State Commun. **100**, 207 (1996).
[21] W. Rieger, T. Metzger, H. Angerer, R. Dimitrov, O. Ambacher, and M. Stutzmann, Appl. Phys. Lett. **68**, 970 (1996).
[22] N. Grandjean, J. Massies, P. Vennègués, M. Laügt, and M. Leroux, Appl. Phys. Lett. **70**, 643 (1997).
[23] D. Kirillov, H. Lee, and J. S. HarrisJr., J. Appl. Phys. **80**, 4058 (1996).
[24] D. D. Manchon, Jr., A. S. Barker, Jr., P. J. Dean, and R. B. Zetterstrom, Solid State Commun. **8**, 1227 (1970).
[25] P. Perlin, C. Jauberthie-Carillon, J. P. Itie, A. S. Miguel, I. Grzegory, and A. Polian, Phys. Rev. B **45**, 83 (1992).
[26] M. A. Nusimovici and J. L. Birman, Phys. Rev. **156**, 925 (1967).
[27] P. Giannozzi, S. de Gironcoli, P. Pavone, and S. Baroni, Phys. Rev. B **43**, 7231 (1991).

[28] A. Debernardi, N. M. Pyka, A. Göbel, T. Ruf, R. Lauck, S. Kramp, and M. Cardona, Solid State Commun. **103**, 297 (1997).
[29] R. Henn, T. Strach, E. Schönherr, and M. Cardona, Phys. Rev. B **55**, 3285 (1997).
[30] C. O. Rodríguez, A. I. Liechtenstein, I. I. Mazin, O. Jepsen, O. K. Andersen, and M. Methfessel, Phys. Rev. B **42**, 2692 (1990).
[31] R. E. Cohen, W. E. Pickett, and H. Krakauer, Phys. Rev. Lett. **64**, 2575 (1990).
[32] D. Strauch, A. P. Mayer, and B. Dorner, Z. Phys. B **78**, 405 (1990).
[33] K. Karch, F. Bechstedt, and T. Pletl, Phys. Rev. B **56**, 3560 (1997).
[34] N. Troullier and J. L. Martins, Phys. Rev. B **43**, 1993 (1991).
[35] I. Gorczyca, N. E. Christensen, E. L. Peltzer y Blancá, and C. O. Rodríguez, Phys. Rev. B **51**, 11 936 (1995).
[36] K. Miwa and A. Fukumoto, Phys. Rev. B **48**, 7897 (1993).